Hybrid Scaled Structural Dynamic Models and Their Use in Damping Prediction

Edward F. Crawley,* Jonathan L. Sigler†, and Marthinus C. van Schoor‡
Massachusetts Institute of Technology, Cambridge, Massachusetts 02139
and
Marc J. Gronet§
Lockheed Missile & Space Company, Sunnyvale, California 94304

Analytical and experimental techniques for the prediction and ground verification of the damped structural dynamics of space structures are developed. The options available for similarity-scaled model testing, including replica and multiple scale approaches, are reviewed. For the case when the distortion of potentially dissipative or nonlinear joints, which would be required in multiple-scale modeling, is impractical, a new type of modeling is introduced, which uses a *hybrid* of joints at replica scale and connecting elements at a modified multiple scale. The model design requirements for replica, multiple-scale, and hybrid models are developed, and the expected scaling of nonlinear dissipation in joints is derived. A damping prediction scheme is developed that relies on a finite element model of the undamped structure and measurements of the individual joint properties to predict the modal damping of the truss attributable to the joints. A hybrid-scaled model of a segment of the space station was built and dynamically tested. The predicted and measured truss damping compared favorably.

Nomenclature

A = cross-sectional area; also used as subscript to λ
c = length correction factor
d = dimension of precompression on gap
e = coefficient of restitution
I = area moment of inertia; also used as subscript to λ
L = length; also used as subscript to λ
P = force; also used as subscript to λ
U = strain energy
u = displacement in x; also used as subscript to λ
v = displacement in y; also used as subscript to λ
η = loss factor
ρ = density; also used as subscript to λ
λ = model scaling factor
μ = coefficient of friction; also used as subscript to λ
θ = rotational displacement; also used as subscript to λ

Subscripts

F = friction
g = overall geometric dimensions
H = hybrid
j = joint
t = tube, time
tot = total (joint plus tube)
k = stiffness
B = bays of truss
δ = linear displacement

Superscripts

. = differentiation with respect to time
' = differentiation with respect to spatial coordinate

Received July 11, 1988; revision received July 27, 1989.

*Associate Professor, Space Engineering Research Center.
†Research Assistant, Space Engineering Research Center.
‡Research Associate, Space Engineering Research Center.
§Research Specialist, Space Station Programs.

Introduction

AEROSPACE dynamicists have traditionally relied on ground vibration testing to span the gap between analytical prediction and in-flight vehicle behavior. Such testing has proven invaluable in gaining a better understanding of complex dynamic phenomena and in developing confidence in analytical models. The approaching era of more flexible and potentially actively controlled space structures imposes additional requirements for both the precision and nature of ground vibration testing, including the requirement of estimation of the on-orbit structural damping.[1] This is especially true in actively controlled structures where the level of passive structural damping directly influences both the robustness and achievable authority of the active controller.[2] Since these factors influence vehicle performance, preflight knowledge of the structural damping becomes a necessity.

The difficulty of testing the next generation of large flexible space structures on the ground places an emphasis on developing innovative means of validating the predicted dynamic behavior.[3] In some cases the large size of the structure prohibits testing the full-scale spacecraft. In other cases, the gravity-induced loads and deflections are excessive. The prediction, and even measurement of damping in such large built-up structures is especially challenging. Although several systematic approaches to damping prediction have been proposed, none has yet been completely verified.[4]

The objective of this research is to develop analytical and experimental techniques to verify the mode shapes, frequencies, and damping in flexible space structures, including those with dissipative and weakly nonlinear joints.

Several options are available for ground testing of a flexible space structure. Among these are component testing, multiple boundary-condition testing[5] of the full-scale structure, and testing of a subscale model of the structure.[6] The first two approaches have the advantage of using full-scale hardware but also require the experimental use of artificial boundary conditions and then the use of an additional step of analytical synthesis. Scale model testing requires the understanding of the linear and nonlinear scaling laws, but tests the entire vehicle as a whole, and is likely the most accurate approach to

predicting structural damping. It is probable that in any major development program a complementary combination of these three approaches would be used.

A wide variety of similarity-scaled models have already been used in the aerospace field.[7] Replica scaling, in which the exact geometric dimensions of all parts are scaled and the model is built of materials identical to those in the full-scale vehicle, is often used. In replica-scale models, there is only one scale factor, designated λ, that is used in various powers to scale all dimensions, stiffnesses, and masses. Aside from common replica scaling, another common technique involves multiple-scale models, which are designed with more than one scale factor. Aeroelastic models, with one scale factor for geometry and a second for velocity, are examples of multiple-scale modeling.[8] In principle, multiple-scale models of space structures could be built.

A multiple-scale model of a truss could, for example, have the overall geometry of a 1/12 scale model but the dynamic behavior of a 1/3 scale model. Such a model would not be a replica model. Structural cross sections, materials, or both, would have to be modified. In practice simple multiple-scale models cannot always be built. There may be parts of the structure, such as nonlinear structural joints, that cannot be modified in material or cross section. These small components must be built in replica at the dynamic scale factor. The nominally linear connecting elements then must be constructed of appropriately modified cross section and material to preserve the overall mass and strain-energy distribution and to give the model the overall dimensions appropriate to the geometric-scale factor. Such a model will be called a hybrid multiple-scale model or simply a hybrid-scale model.

The first objective of this paper is to derive the scaling laws and other requirements that must be met to construct such a hybrid-scale, structural, dynamic model that includes joints. Such a model of a 1/12 geometric scale, 1/3 dynamic scale, seven-bay section of the proposed space station truss was then designed. Two nominally identical models were built and tested: a control model, which did not have quick connect joints.

The second objective of the paper is to determine if the structural damping due to the joints in such a truss structure can be accurately predicted a priori from a knowledge of the properties of the joints and other structural elements. The methodology for such a prediction will first be reviewed. The measured properties of the joints will then be used to predict the differences in the structural damping of the first three modes of the two test articles. The predicted and measured modal damping will then be compared.

Dynamic Scaling Laws

Similarity Scaling for Undamped Truss Dynamics

In this section we will develop the scaling laws pertinent to replica, multiple, and hybrid-scale structural dynamic models and then examine how the structural damping is affected in these scaling options. The structure of interest is assumed to be a frame truss made up of struts consisting of relatively short joints and relatively long and slender tubes. A simplified matrix model equation can be developed[7] for this structure:

$$\rho AL\ddot{v} + \frac{EA}{L}(u + v) + \frac{EI}{L^3}(u + v) + \frac{EI}{L^2}\theta = P_y \qquad (1)$$

where u and v are the deflections and θ the rotations in the plane of the truss. In this equation, as in all equations in this section, the meaning of the positive and equal signs should be interpreted as being correct to an arbitrary, unspecified, numerical constant. The potentially independent scale factors in Eq. (1) are $\lambda_{\rho A}$, λ_L, $\lambda_u = \lambda_v = \lambda_\delta$, λ_t, λ_{EA}, λ_{EI}, λ_θ, λ_P. To preserve the kinetic energy distribution (first term), strain energy distribution (second, third, and fourth terms), and forced response behavior (final term), the five terms of Eq. (1) must have the same dimensions, requiring that

$$\lambda_{\rho A}\lambda_L\lambda_\delta\lambda_t^{-2} = \lambda_{EA}\lambda_L^{-1}\lambda_\delta = \lambda_{EI}\lambda_L^{-3}\lambda_\delta = \lambda_{EI}\lambda_L^{-2}\lambda_\theta = \lambda_P \qquad (2)$$

Multiplying the terms of Eq. (1) by corresponding terms in Eq. (2) simply converts Eq. (2) in full-scale quantities, into the identical equation for the model-scale counterparts. If the requirements of Eq. (2) are met, the model will have the same mode shapes and the correct scale frequency and deflections when compared to the full-scale article. Note that the scale factor for the linear *deflections* has not necessarily been assumed to be the same as the scale factor for the linear *dimensions*.

In general similarity scaling, the scale factors for time, length and mass, or any three quantities whose dimensions uniquely span time, length, and mass, are selected. Scale factors for the remaining derived quantities are then determined in terms of these three primary factors. In this derivation, the possibility for choosing two independent length scales, one for geometry and one for the deflections, will be maintained. This leads to the possibility of choosing four primary-scale factors.

Replica Scaling

In replica scaling, the length scale factor is chosen as the fundamental dynamic scale factor $\lambda_L = \lambda$. Additional requirements that all dimensions and deflections are scaled by this scale factor and that the same materials are used as in the full-scale article are imposed. This implies that the four primary scale factors are uniquely set to be

$$\lambda_L = \lambda \quad \lambda_{\rho A} = \lambda^2 \quad \lambda_{EA} = \lambda^2 \quad \lambda_\delta = \lambda \qquad (3)$$

These primary-scale factors are shown as the underlined entries in Table 1, and the derived quantities are listed in Tables 1 and 2. Note in particular that angles (and strain) are preserved, that loads scale as λ^2, and time (frequency)$^{-1}$ as λ.

Length/Frequency-Force-Displacement Multiple Scaling

There is some minimum value of the replica scale factor λ below which replica scaling becomes impractical. The components become too fragile, are at minimum gauge, or are too difficult to machine accurately. If it is necessary to reduce the size of the model below this limit, a possible alternative is multiple-factor scaling. In this version, the objective is to have the frequencies, forces, and displacements be those of an equivalent replica model of scale factor λ as the model is built at a smaller, geometric scale factor λ_g. Enforcing these requirements, the four primary scale factors become

$$\lambda_L = \lambda_g \qquad \lambda_\delta = \lambda \qquad \lambda_t = \lambda \qquad \lambda_P = \lambda^2 \qquad (4)$$

Note that in this type of model the dimensions scale as λ_g, but the deflections scale as λ. The remaining derived quantities are given in terms of these primary scale factors in Tables 1 and 2. In such a model, not only are the frequency, force, and displacement that of an equivalent replica model, but so are the mass and the work done by forces and moments, and the strain and kinetic energies. Thus, the linear components of the mode shapes and deflections under load will all be the same as for a replica model at scale-factor λ.

What are the design implications for such a model? First, that the cross section of the struts must be modified. Since $\lambda_{EA} = \lambda\lambda_g$ and $\lambda_{EI} = \lambda\lambda_g^3$, the I/A of the strut must change like λ_g^2. For a thin wall tubular strut, this is easily done by maintaining the wall thickness and changing the radius. For thicker wall tubes and solids there are some additional constraints. Also since $\lambda_{\rho A} = \lambda^3\lambda_g^{-1}$, the E/ρ of the material must change like $\lambda^{-2}\lambda_g^2$. This may require either a change in material and/or the addition of nonstructural mass. It should be noted that in length/frequency-force-displacement (L/FFD) scaling, the angles of deformation are not preserved, but scaled as $\lambda_\theta = \lambda\lambda_g^{-1}$.

Table 1 Primary and important derived scaling factors[a]

Scaling factor	Replica scaling[b]	L/FFD scaling	L/FFS scaling
$\lambda_{\rho A}$	$\underline{\lambda^2}$	$\lambda^3\lambda_g^{-1}$	$\lambda^4\lambda_g^{-2}$
λ_{EA}	$\underline{\lambda^2}$	$\lambda\lambda_g$	λ^2
λ_{EI}	λ^4	$\lambda\lambda_g^3$	$\lambda^2\lambda_g^2$
λ_L	$\underline{\lambda}$	$\underline{\lambda_g}$	$\underline{\lambda_g}$
λ_δ	$\underline{\lambda}$	$\underline{\lambda}$	$\underline{\lambda_g}$
λ_θ	$\underline{1}$	$\lambda\lambda_g^{-1}$	$\underline{1}$
λ_t	λ	$\underline{\lambda}$	$\underline{\lambda}$
λ_P	λ^2	$\underline{\lambda^2}$	$\underline{\lambda^2}$
λ_d	λ	λ	λ_g
λ_μ	1	1	1
λ_e	1	1	1

[a]Primary factors are underlined.
[b]Also applies to joints in hybrid scaling.

Table 2 Additional derived scaling factors

Scaling factor	Defining relation	Replica scaling	L/FFD scaling	L/FFS scaling
Frequency	λ_t^{-1}	λ^{-1}	λ^{-1}	λ^{-1}
Moment	$\lambda_P\lambda_L$	λ^3	$\lambda^2\lambda_g$	$\lambda^2\lambda_g$
Linear velocity	$\lambda_\delta\lambda_t^{-1}$	1	1	$\lambda^{-1}\lambda_g$
Linear acceleration	$\lambda_\delta\lambda_t^{-2}$	λ^{-1}	λ^{-1}	$\lambda^{-2}\lambda_g$
Angular velocity	$\lambda_\theta\lambda_t^{-1}$	λ^{-1}	λ_g^{-1}	λ^{-1}
Angular acceleration	$\lambda_\theta\lambda_t^{-2}$	λ^{-2}	$\lambda^{-1}\lambda_g^{-1}$	λ^{-2}
Axial stiffness, k_{uu}	$\lambda_{EA}\lambda_L^{-1}$	λ	λ	$\lambda^2\lambda_g^{-1}$
Bending stiffness, k_{vv}	$\lambda_{EI}\lambda_L^{-3}$	λ	λ	$\lambda^2\lambda_g^{-1}$
Bending stiffness, $k_{v\theta}$	$\lambda_{EI}\lambda_L^{-2}$	λ^2	$\lambda\lambda_g$	λ^2
Bending stiffness, $k_{\theta\theta}$	$\lambda_{EI}\lambda_L^{-1}$	λ^3	$\lambda\lambda_g^2$	$\lambda^2\lambda_g$
Strain energy		λ^3	λ^3	$\lambda^2\lambda_g$
Total mass	$\lambda_{\rho A}\lambda_L$	λ^3	λ^3	$\lambda^4\lambda_g^{-1}$
Static imbalance	$\lambda_{\rho A}\lambda_L^2$	λ^4	$\lambda^3\lambda_g$	λ^4
Moment of inertia	$\lambda_{\rho A}\lambda_L^3$	λ^5	$\lambda^3\lambda_g^2$	$\lambda^4\lambda_g$
Kinetic energy		λ^3	λ^3	$\lambda^2\lambda_g$
Local global frequency	$(\lambda_{EI}\lambda_{EA}^{-1}\lambda_L^{-2})^{1/2}$	1	1	1
Buckling margin	$\lambda_P\lambda_L^2\lambda_{EI}^{-1}$	1	$\lambda\lambda_g^{-1}$	1
Gravity deformation	$\lambda_{\rho A}\lambda_L\lambda_P^{-1}$	λ	λ	$\lambda^2\lambda_g^{-1}$

Length/Frequency-Force-Strain Multiple Scaling

In this slight variation from the previous section, the frequency, force, and *strain* (in contrast to displacement) are set to their values in an equivalent replica model, but the overall dimensions still scale as λ_g. With these requirements,

$$\lambda_L = \lambda_g \qquad \lambda_\delta = \lambda_g \qquad \lambda_t = \lambda \qquad \lambda_P = \lambda^2 \tag{5}$$

and the remaining derived quantities are given in Tables 1 and 2. In this version of multiple scaling, the linear and rotational deflection aspects of the mode shapes are preserved, but the magnitude of the linear deflections is λ_g, and the kinetic and potential energy are $\lambda^2\lambda_g$, slightly different from their value in a replica-scale model. The advantage of this version is that the rotational deformations are correctly scaled.

The dependence of three additional practical test considerations are listed for similarity-scaled models at the bottom of Table 2. The local/global frequency ratio is a measure of when the local transverse vibration of the struts will become important to the overall dynamics. It scales as unity for all three cases. The buckling margin is favorable and, of course, the structural Froude number (the ratio of gravity to stiffness influences) always diminishes with scale.

Hybrid Scaling

If only the bulk cross-sectional properties of a structural element (dimensions, shape, density) influence the dynamics of the structure, then the scaling laws already derived can be used to design modified cross sections appropriate for a multiple-scale model. However, there are sometimes localized elements such as joints and connections that have complex load paths, nonlinearities, or dissipation characteristics, which cannot be simulated by a modified cross section. These elements must be built in replica scale at the dynamics-scale factor λ. The resulting combination of a multiple-scale model, which incorporates small replica elements, is called a hybrid-scale model.

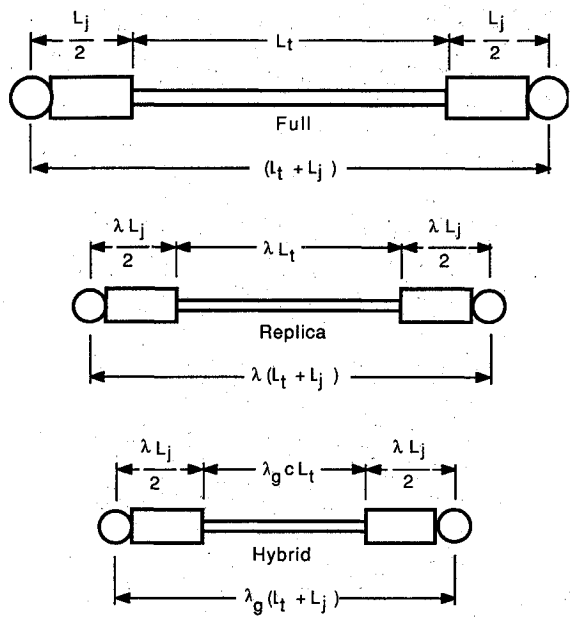

Fig. 1 Dimensions of a joint-tube-joint strut in full (top), replica (middle), and hybrid (bottom) scale.

An example of a hybrid model is shown in Fig. 1. In going from full scale to replica scale, all dimensions are scaled exactly by λ. In going from replica to hybrid scale, the joints have been kept at replica scale λ, but the overall geometry of the strut has been reduced to that of λ_g. Since there are two types of multiple-scale models, there are two corresponding options for hybrid-scale models. One incorporates replica joints into an L/FFD multiple scale model, and is designated hybrid length/frequency-force-displacement (HL/FFD) modeling. The second combines replica joints with a length/frequency-force-strain (L/FFS) multiple-scale model and is designated hybrid length/frequency-force-strain (HL/FFS) modeling.

In such a hybrid-scale model, the presence of the small replica joint slightly changes the scaling factors for the connecting tubes. Four constraints must be met by the tube to give the total strut the correct multiple scale properties, while maintaining the joints at replica scale. The first is that the total length of the strut must scale with the multiple-scale model factor, whereas the joint length scales with the replica scale

$$L_{\text{tot }H} = \lambda_g L_{\text{tot}}$$
$$L_{jH} = \lambda L_j \tag{6}$$

Examining Fig. 1 and introducing the length correction factor c gives

$$\lambda_g c L_t + \lambda L_j = \lambda_g (L_t + L_j) \tag{7a}$$

or

$$c = 1 + \left(\frac{\lambda_g - \lambda}{\lambda_g}\right)\frac{L_j}{L_t} \tag{7b}$$

The second constraint is that the total mass of the hybrid tube plus joint is scaled by the appropriate multiple-scale factor (row 1, column 2 or 3 of Table 1)

$$[(\rho A)L]_{\text{tot }H} = \lambda_{\rho A}\lambda_g[(\rho A)L]_{\text{tot}} \tag{8a}$$

$$[(\rho A)L]_{jH} = \lambda^2\lambda[(\rho A)L]_j \tag{8b}$$

and the joint mass is scaled by the replica-scale factors (row 1, column 1 of Table 1). Since the total mass is just the sum of the mass of the tube and joints, Eq. (8) can be solved for the mass-scale factor of the tube. The results for this and other scaling factors of the tube cross-sectional properties are shown in Table 3.

The third and fourth constraints on the tubes are that the extensional and bending stiffnesses of the hybrid strut are scaled by the appropriate factors, which are listed as the stiffness scaling factors in rows 7–10 of Table 2. The form of the constraint is the same as for the aforementioned length and mass; i.e., that the total strut (joints and tube) stiffness scale by the appropriate multiple-scale factor

$$k_{\text{tot }H} = \lambda_k\, k_{\text{tot}}$$

$$k_{jH} = \lambda_{kj}\, k_j \tag{9}$$

and the joint stiffness is appropriate to replica scale. Unfortunately, the stiffness of a strut consisting of a joint, tube, and joint is not simply the numerical sum of the stiffnesses but also depends on the geometry. It is therefore necessary to derive explicit expressions for the total strut stiffness, as would be measured at the ends of the strut in terms of the joint and tube properties.

This is done by deriving a three-element, finite element model of the strut. The interior nodes, at the joint/tube interface are then statically condensed out, giving only a 2×2 (extension), or 4×4 (bending) stiffness matrix of a planar strut. The final step is to assume that the joint is much stiffer than the tubes and to use binomial expansions to retain first-order corrections. With these assumptions, the various entries in the stiffness matrix of the strut can be expressed as[9]

extension (k_{uu}):

$$\left(\frac{EA}{L}\right)_t\left(1 - \frac{EA_t}{EA_j}\frac{L_j}{L_t}\right) \tag{10a}$$

bending:

$$\left(\frac{EI}{L^a}\right)_t\left(1 - \frac{aEI_t}{EI_j}\frac{L_j}{L_t}\right) \tag{10b}$$

where $a = 3$ for k_{vv}, 2 for $k_{v\theta}$, and 1 for $k_{\theta\theta}$.

These entries are to be interpreted in the following way. Any entry of the stiffness matrix of the strut that relates an extensional deflection to an extensional force can be expressed in terms of the stiffness of the tube $(EA/L)_t$ modified by the second term in parentheses in Eq. (10a). Entries that relate a transverse linear force to a transverse bending deflection (k_{vv}) can be expressed in terms Eq. (10b) with a set to 3, and so forth.

With the strut stiffnesses of Eq. (10), the constraints of Eq. (9), and the stiffness scaling factors of rows 7–10 of Table 2, the stiffness scaling factors for the tube properties can be determined. They are shown in Table 3 for HL/FFD and HL/FFS hybrid scaling. Note that there are three conflicting scaling factors for *EI*. This is because the different entries in the bending stiffness matrix depend on length raised to various orders, and the ratio of the joint-to-tube length has been altered in the hybrid-scale strut. For cases when the joint length is small compared to the tube length, the difference in the three-scale factors for *EI* is small. In design, the average value would probably be used. As a practical matter, the vast majority of strain energy in long, slender struts is stored in extension, and so this small discrepancy in bending stiffness would be relatively unimportant.

So far the requirements necessary to ensure the correct undamped dynamics in five scaled models (replica, L/FFD, L/FFS, HL/FFD, and HL/FFS) have been derived. In the next section, we will examine the degree to which the dissipative effects are preserved in these various scaling options.

Scaling of Damping

Sources of Damping

In any structure in space, there are two major sources of passive damping, material damping, and interface or structural damping. A complete discussion of the scaling of material damping is beyond the scope of this article. The second and probably principal source of structural damping occurs at the joints and interfaces. A general manner in which to characterize such potentially nonlinear dissipation sources is in terms of the loss factor

$$\eta = \frac{\Delta U}{2\pi U} \tag{11}$$

If this quantity is invariant to scaling, then the structural damping due to joints measured in a model will be the same as that in the full-scale structure. From Table 2, it is already known how the strain energy term in the denominator scales for the replica and hybrid models, therefore only the numerator must be examined.

Since no completely generalizable model of joint damping exists, several examples have been examined (see Fig. 2). These include a slipping rotary frictional pin joint, a slipping extensional frictional joint, and a dead-band impacting joint. Each is in some way typical of phenomena that have been observed or are expected in space structure joints.[10]

The scaling of the dissipative behavior of the three joints is derived in detail in the Appendix and is summarized in Table 4. One column expresses how the loss ΔU would scale if the joint does not stick but moves in such a way that the micromotion of the joint is the same as the overall motion of the structure. A second "motion" column shows how the micromotion scales if sticking occurs. If the motion column entry is unity, then the total dissipation scales, as is shown in the ΔU

Table 3 Scale factors for tubes in hybrid scaled models

	HL/FFD hybrid scaling	HL/FFS hybrid scaling
λ_L	$\lambda_g c$	$\lambda_g c$
$\lambda_{\rho A}$	$\lambda^3\lambda_g^{-1}c^{-1}$	$\lambda^4\lambda_g^{-2}c^{-1}[1 + r_{\rho A}(1 - \lambda^{-1}\lambda_g)]$
λ_{EA} (k_{uu})	$\lambda\lambda_g c$	$\lambda^2 c[1 - r_{EA}(1 - \lambda\lambda_g^{-1})]$
λ_{EA} (k_{vv})	$\lambda\lambda_g^3 c^3[1 - 3r_{EI}(1 - \lambda_g^2 c^2\lambda^{-2})]$	$\lambda^2\lambda_g^2 c^3[1 - 3r_{EI}(1 - \lambda_g^2 c^2\lambda^{-1})]$
λ_{EI} $(k_{v\theta})$	$\lambda\lambda_g^3 c^2[1 - 2r_{EI}(1 - \lambda_g^2 c\lambda^{-2})]$	$\lambda^2\lambda_g^2 c^2[1 - 2r_{EI}(1 - \lambda_g c\lambda^{-1})]$
λ_{EI} $(k_{\theta\theta})$	$\lambda\lambda_g^3 c[1 - r_{EI}(1 - \lambda_g^2\lambda^{-2})]$	$\lambda^2\lambda_g^2 c[1 - r_{EI}(1 - \lambda_g\lambda^{-1})]$

with $c = 1 + [(\lambda_c - \lambda)\lambda_c^{-1}]L_j L_t^{-1}$ $r_{\rho A} = \rho A_t L_j(\rho A_j L_t)^{-1}$
$r_{EA} = EA_t L_j(EA_j L_t)^{-1}$ $r_{EI} = EI_t L_j(EI_j L_t)^{-1}$

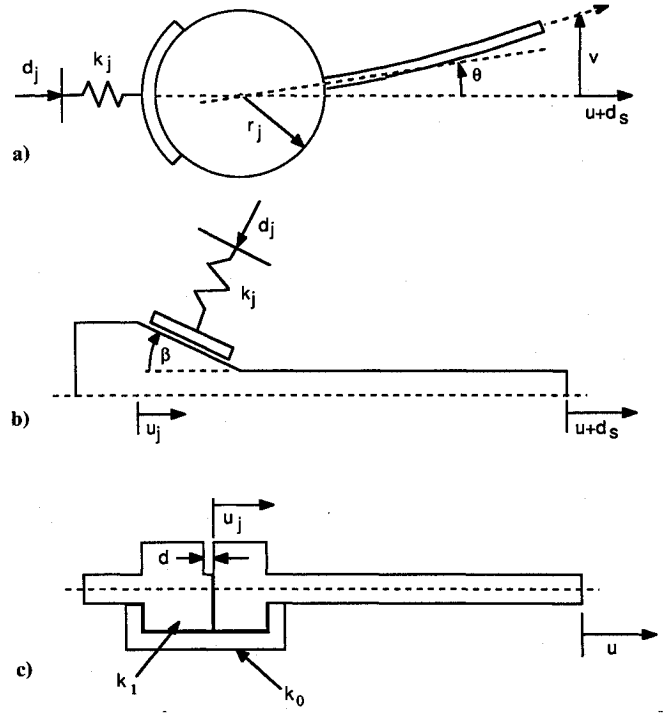

Fig. 2 Three conceptual models of dissipation in joints: a) friction at a rotating pin, b) friction in an axial joint, c) deadband/impacting in an axial joint.

Table 4 Scale factors for the dissipative characteristics of joints

	Replica scaling		L/FFD scaling		L/FFS scaling	
	ΔU	Motion	ΔU	Motion	ΔU	Motion
Pin friction						
Geometric[a]	λ^3	1	$\lambda^4\lambda_g^{-1}$	$\lambda\lambda_g^{-1}$	λ^3	$\lambda\lambda_g^{-1}$
Gravity	λ^4	λ	$\lambda^5\lambda_g^{-1}$	$\lambda^2\lambda_g^{-1}$	$\lambda^5\lambda_g^{-1}$	$\lambda^3\lambda_g^{-2}$
Axial friction						
Geometric	λ^3	1	λ^3	1	λ^3	1
Gravity	λ^4	λ	λ^4	λ	$\lambda^5\lambda_g^{-1}$	$\lambda^2\lambda_g^{-1}$
Dead band	λ^3	——	λ^3	——	$\lambda^4\lambda_g^{-1}$	——

[a] Effects due to geometric preload in the joint, tolerance in strut length, and displacement dependent friction

column. If the motion column is other than unity, then the dissipation can scale at functional powers of λ and λ_g equal to or greater than those shown in the ΔU column, but less than or equal to the product of the motion times ΔU columns. For the two frictional joints, there are also two rows, one that shows how the gravity-load-induced frictional dissipation scales and one that shows how the dissipation due to all other sources of load scales. The gravity-induced terms always show a Froude number effect and scale with a higher power of λ than the other effects. Implicit in these scaling factors are the assumptions that the surface friction μ and tolerances d scale as shown in the ninth and tenth rows of Table 1.

Aside from friction, a second common nonlinear dissipative mechanism is dead band/impacting, or "slop." A model of this is shown in Fig. 2c. Two preloaded surfaces are in imperfect contact, such that over part of a cycle of motion the gap closes, and over the remainder of the cycle it is open. At the point of contact the stiffness of the joint changes, and a small amount of energy is dissipated due to the impact. The process of dissipation is complex and depends on the local geometry and material properties. For simple collisions, one measure of dissipation is the coefficient of restitution, a measure of the fraction of initial velocity retained after collision. If the coefficient of restitution e is held fixed (last row of Table 1), then the energy dissipated in impact scales, as shown in the last row of Table 4.

Design Implications

Examining the dissipative characteristic of joints as summarized in Table 4, we observe that for replica scaling all nongravitationally induced dissipative effects scale as λ^3. Since the strain energy also scales as λ^3, Eq. (11) implies that the loss factor will be independent of scale. For L/FFD multiple (and HL/FFD) scaling, the nongravitational axial friction and losses from impact also scale as λ^3. For L/FFS multiple (and HL/FFS) scaling, the scaling of losses is more complex.

Based on the derivation of the undamped dynamic and damping scaling laws, as summarized in Tables 1–4, the following design implications can be drawn.

If model tolerances are scaled by λ, and friction and restitution coefficients in the joints are unchanged, then a replica model of a space structure will perfectly represent the dynamics, including the influences of all postulated sources of joint nonlinearity and damping. The exception is that all the influences of gravity are reduced in smaller-scale models.

If the primary source of strain energy storage and joint nonlinearity is *axial* deformation of the struts, then an HL/FFD model (which does not correctly reproduce angular deformations) will correctly reproduce the *displacement* mode shapes, amplitudes of forced response, and damping of the full-scale article.

If the strain energy storage and/or dissipation involves significant bending or angular deformation, then an HL/FFS model will correctly reproduce the mode shapes, *strain* amplitudes of forced vibration, and the dissipation of frictional loss mechanism. Because most of the losses scale as λ^3, and strain energy as $\lambda^2\lambda_g$, Eq. (11) indicates that the loss factor (and critical damping ratio) will scale as $\lambda\lambda_g^{-1}$.

Thus when designing a hybrid-scale model, it will sometimes be beneficial to use HL/FFD scaling and sometimes HL/FFS scaling.

Truss Damping Experiment

Specimen Design

Having established that hybrid-scaled models can be used to assess the structural damping in jointed space structures, an experimental test program was then undertaken. The objective of this program was twofold: to experimentally measure the contribution of the joints to the structural damping and to validate the damping synthesis procedure to be discussed. Because of its timeliness, a section of the box truss to be used in the Space Station Freedom was chosen as the test article.

The central issue in the design of the test specimens is how to isolate the contribution of the joints to the damping. It was decided to build two test articles. A jointed model (see Fig. 3) was built that incorporated one complete bay of Star*Net quick-connect joints (Space Structures Inc., Plainview NY), prototypical of the ones that might be used on the space station. A control model without the joints was also built. By comparing the difference in measured damping between the two, the influence of material, aerodynamic, and support damping would nominally be eliminated.

The Star*Net quick-connect joint is designed to be easily assembled in space (see Fig. 4). A locking ring is twisted to compress a segmented ring, which preloads the sloping contact surfaces, driving the normal mating faces into contact. The joint is available in replica scales down to 1/4 and has been tested in full- and subscale,[11,5] indicating that 1/3-scale models retained the scaled stiffness and damping of the full-scale joint.

An L/FFD hybrid model was the preferred type of scaled test article. A hybrid model was required because, at 1/3 replica scale, only one bay of the 5-m space station structure would fit in the 10-ft-diam MIT ASTROVAC vacuum test facility. Since the most probable loss mechanism in the

Star*Net joint is axial friction, and since space station struts are sufficiently slender that they essentially store only axial strain energy, a seven-bay HL/FFD hybrid model ($\lambda = 1/3$, $\lambda_g = 1/12.7$) was selected.

The actual detail design of the test articles was the result of a great deal of iteration. The pertinent properties of the actual space station are listed in Table 5. The current baseline space station struts are 2-in. o.d., 0.1-in. wall thickness graphite/epoxy tubes. The scaled properties of a 1/3 replica model, as are the ideal properties of a 1/3—1/12.7 HL/FFD model. The hybrid properties are calculated using the factors of Table 3, with $c = 0.645$, assuming $EI_j = EI_{ht}$ and averaging the three conflicting scale factors for EI. The design challenge is to meet these goals. It was found that a 0.374-in. o.d., 0.037 in. wall thickness aluminum tube came close to meeting the EA requirement. The aluminum tube is about a factor of 6 too light, which was compensated for by adding mass at the nodes, and a factor of 10 too stiff in bending. Because of the slenderness of the tubes, the extra bending stiffness was found analytically to not change the modal characteristics of the truss.

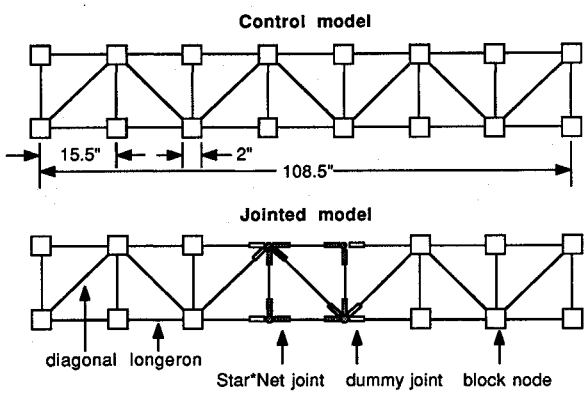

Fig. 3 Control and jointed bay-test articles.

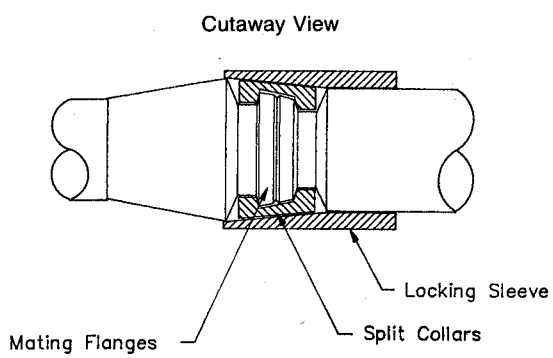

Fig. 4 Star*Net quick connect joint.

For reasons of economy, only the central bay of the jointed test article was outfitted with Star*Net joints. At the other nodes of the jointed article, and all nodes of the control article, a simple joint was needed. The joint used was a 2-in. cube of aluminum, bored with 0.75-in. deep 0.380-in. diam holes. The tubes were then bonded to these joints with a 0.003-in. thick bond line of 3M #2216 B/AA room temperature cure epoxy.

Finite Element Analysis

A STRUSAP finite element model of the seven-bay truss was developed. The model included one 12-degree-of freedom cubic assumed displacement beam element for each strut. The joint and node stiffnesses were statically condensed out to determine an effective modulus for the entire strut.

The frequencies for the first three modes, two bending modes and a torsion mode, are listed in Table 6. The resonant frequencies of the jointed article are slightly higher due to the additional stiffness in the central bay. The mode shapes of the control model are shown in Fig. 5. The jointed model modes are qualitatively similar. The close proximity of bending and torsion modes and the shape of the bending mode, indicate that the "bending" motion is primarily one of the truss bays shearing. The 10% difference in predicted vs measured frequency of the first mode can be attributed to the flexibility of the joints.

Dynamic Testing

The test articles were suspended and tested in such a way as to match as closely as possible the weightlessness and vacuum of space. The specimens were suspended by two 18-in. lengths of 0.026-in. steel piano wire from a heavy overhead structure in the MIT ASTROVAC.[12] The wires were attached to the third and sixth of the eight nodes along one edge to minimize their contribution to the model stiffness. Since the first frequency of the support wires was 180 Hz, well above the test range, little transmission of energy out of the test article through the suspension was expected. The tests were conducted in 1 Torr vacuum to eliminate air drag and using a single inertial shaker. The structure was thus completely isolated except for the two suspension wires and light instrumentation cabling.

The model was excited using a sine sweep technique by a single rotary dc shaker mounted at one end of the structure. Acceleration was measured at the opposite end and at a support point, and strain was measured in the lower central longeron. Constant input amplitude sine sweeps were conducted about the first three modal frequencies for three levels of peak longeron force: low (2–4 lb amplitude), medium (10 lb), and high (20 lb). This corresponds to full-scale forces of 18–36 lb, the nominal operating range for the space station, 90 lb and 180 lb, respectively.

As shown in Table 6, the first three modes were found at 70, 80, and 93 Hz for the control-test article and 73, 86, and 96 Hz for the jointed test article. All are in reasonable agreement

Table 5 Space station and model characteristics

Quantity	Full-scale station	1/3-scale replica	Ideal 1/3, 1/12.7 HL/FFD	Actual 1/3, 1/12.7 HL/FFD
L_t (in.)	177.50	59.17	9.01	9.00
L_j (in.)	19.50	6.50	6.50	6.50
r_t, in.	1.000	0.333	—	0.187
t_t, in.	0.100	0.033	—	0.037
A_t, in.^{2}	0.5969	0.0664	—	0.03917
I_t, in.^{4}	0.2701	0.0033	—	0.000563
ρ_t, lb/in.^{3}	0.055	0.055	—	0.097
E_t, Mlb/in.^{2}	36.0	36.0	—	10.00
ρA_t lb/in.	0.0328	0.00365	0.0239	0.0038
EA_t, Mlb	21.5	2.39	0.363	0.392
EI_t, Mlb in.^{2}	9.72	0.120	0.00057[a]	0.00563

[a] Average of (0.00028, 0.00052 and 0.00091).

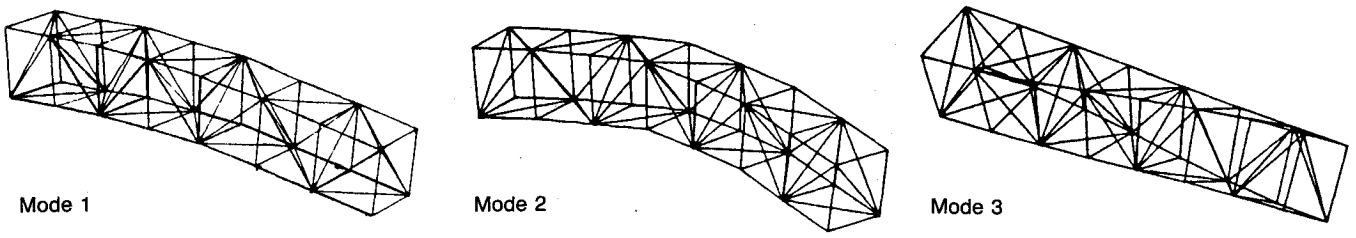

Fig. 5 First three mode shapes as predicted by finite element analysis.

Table 6 Predicted and measured model modal dynamics

	Predicted		Measured			
	Frequency, Hz	ζ, %	Frequency, Hz	ζ, %		
Jointed model				Low	Med	High
Mode 1	82	——	73	0.19	0.14	0.19
Mode 2	82	——	86	0.19	0.14	0.13
Mode 3	90	——	96	0.18	——	——
Control model						
Mode 1	79	——	70	0.12	0.17	0.12
Mode 2	79	——	80	0.10	0.14	——
Mode 3	89	——	93	0.12	——	——
Difference						
Mode 1	3.0	0.04	3.0	0.07	−0.03	0.07
Mode 2	3.0	0.04	6.0	0.09	0.00	——
Mode 3	1.0	0.03	3.0	0.06	——	——

with the finite element model. The splitting of the two bending modes is thought to be due to unmodeled asymmetry in the truss.

In the damping tests, the first mode was tested at low, medium, and high forcing levels, the second mode, at low and medium, and the third was tested only at low levels. Measured damping ratios are given in Table 6. The damping in both specimens is quite low, averaging between 0.1% and 0.2% in critical damping ratio ζ. The damping measurements were repeatable within a 0.02% critical damping ratio tolerance range. The material damping of the aluminum alone would be expected to contribute up to 0.1% in ζ, and so the joints contribute very little damping. The difference in the measured damping; i.e., the damping attributable to the joints, is also shown in Table 6. In four of the six modes and force levels there was a measurable increase in damping. In one case the damping in the jointed article is less, and in one case there is no change. If these latter two cases are not included, the average $\Delta\zeta$ is 0.073%. If they are included, the average is 0.043%. Therefore, the additional damping due to the joints is concluded to be 0.04% to 0.08% in ζ corresponding to a difference in loss factor $\Delta\eta$ of 0.08% to 0.16%.

Damping Prediction

Damping Synthesis

Now that a small difference in the damping of the jointed and control test articles has been measured, there remains the question of whether this magnitude of structural damping can be predicted from a knowledge of the individual joint behavior. A scheme for such a prediction includes three steps: the development of a synthesis approach; the collection of data on the joint properties; and the incorporation of this data into the synthesis approach and correlation with actual measurements.

Several comprehensive damping synthesis approaches have been proposed.[13] The one to be employed here is based on the determination of the structural loss factor [Eq. (11)], which for a built-up structure can be written

$$\eta = \sum \Delta U_k / 2\pi \sum U_i \tag{12}$$

where the upper sum is over all k dissipative elements, and the lower sum is over all i strain energy storage elements.[4] For lightly damped structures, it can be assumed that the mode shapes are real and closely resemble the mode shapes of the undamped structure. From the undamped, finite element analysis, the modal strain energy can be determined. The only additional information needed is the function that expresses the energy loss for each dissipative element. The information usually measured and reported is the dissipative element loss factor η_k. Again using Eq. (11), the energy loss for the kth element can be expressed as

$$\Delta U_k = 2\pi U_k \eta_k(P) \tag{13}$$

where U_k is the strain energy stored in the dissipative element and $\eta_k(P)$ is the load (P) dependent loss factor. The possibility of load dependence of the element loss factor has been explicitly shown. Substituting into Eq. (12) gives a general expression for the structural loss factor

$$\eta = \sum U_k \eta_k(P) / \sum U_i \tag{14}$$

For the special case of light damping, such that the complementary and potential strain energy are nearly equal and the mode shapes are nearly real, and for the case where the loads and dissipative effects are primarily axial, then the strain energy in a joint is just

$$U_j = \frac{P^2}{2k_j} = \frac{(EA)_i^2 \epsilon_i^2}{2k_j} \tag{15}$$

and the loss factor for a truss in which each strut has two joints, and in which the tubes store most of the strain energy is

$$\eta = \frac{2\sum \left[\frac{\eta_j}{k_j} (EA)_i^2 \epsilon_i^2 \right]_k}{\sum [(EA)_i \epsilon_i^2 L_i]_i} \tag{16}$$

Eq. (16) is the one that will be used to correlate the joint data with the actual truss damping measurements. It is clear that all

the information necessary to compute the structural loss factor is available in a conventional finite element analysis, except for the stiffness and loss factor of the joints.

To develop some physical insight for "back of the envelope" estimates, a useful simplification of Eq. (16) can be derived for the case in which the truss properties are uniform, the strain distribution is uniform and primarily carried in the longerons, and the joint loss factor is independent of load. Then the truss loss factor is

$$\eta \cong \frac{N_j}{N_B}\frac{\eta_j}{k_j}\left(\frac{EA}{L}\right)_t \tag{17}$$

where N_j is the number of joints in any longeron of the truss, and N_B is the number of bays. Stiffer truss tubes and increased dissipation in the joints will increase truss damping, whereas truss damping will decrease for an increase in the number of truss bays and joint stiffness.

Measured Joint Properties

The mechanical properties of the Star*Net joint have been independently measured by three laboratories: NASA Langley Research Center,[11] CSA Engineering, Inc.,[14] and Massachusetts Institute of Technology.[9] In all three laboratories, conventional, quasistatic, force-stroke measurements were made, and the damping inferred by the hysteretic behavior. At CSA and MIT, force-state measurements were also made. In force-state measurements, the joint is driven by a dynamic shaker, and the force is correlated in terms of both displacement and velocity; i.e., the mechanical state of the joint.[10]

The test setup in the three laboratories also differed considerably. At Langley Research Center and CSA the joints were cycled in conventional hydraulic test machines. In both of these tests, the support fixtures were extremely rigid as the primary objective of the tests was to measure stiffness. In the MIT force-state tests, load was applied by an electrodynamic shaker. In the MIT quasisteady tests, a manually operated winch and compliant link were used to allow smooth application of load at very small levels.

Considering these differences in test procedures, the variability of the joints, and the uncertainty of testing at different scales, the three tests produced results in reasonable agreement. In the CSA tests, performed on a two-sided (joint-node-joint), full-scale joint, a stiffness of 338,000 lb/in. and a loss factor well less than 1% were measured. Corrected to a one-sided, 1/3-scale condition, this gives $k_j = 225{,}000$ lb/in. and $\eta_j < 0.01$. The Langley Research Center tests, conducted on a two-sided, 1/3-scale joint, yielded a stiffness of 100,000 lb/in. and a lower confidence estimate of loss factor of about 2%. Corrected, these give $k_j = 200{,}000$ lb/in. and $\eta_j = 0.02$. The MIT tests were performed on a one-sided, 1/3-scale joint. The stiffness measured was $k_j = 96{,}000$ lb/in. The loss factor as a function of load is shown in Fig. 6. The minimum loss measured was $\eta_j = 0.003$. Higher loss factors at low loads are thought to be due to poor signal to noise. Comparing the three, the CSA and Langley measured stiffnesses are in essential agreement. It is likely that unmodeled compliance in the test fixture caused the MIT stiffness measurement to be too low. Correcting the MIT measured stiffness to the 200,000 lb/in. range has the effect of doubling the measured loss factor. This causes the MIT and CSA loss factors to be in essential agreement at $\eta_j = 0.01$. For the purposes of damping prediction, the highest confidence estimates of $k_j = 225{,}000$ lb/in. and $\eta_j = 0.01$ will be used. Since the dependence of loss on load is not strong over the operating range of 5-25 lb, it will be ignored.

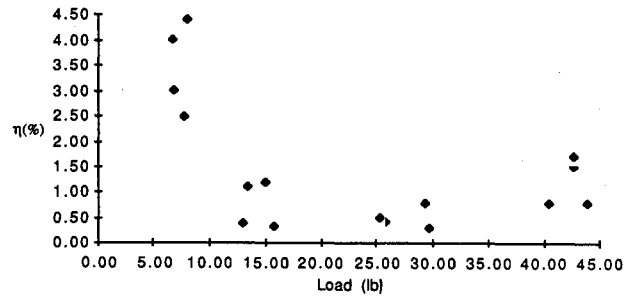

Fig. 6 Loss factor vs maximum load for joints *A* and *B*.

Truss Damping Prediction

Finally, we are in a position to predict the difference in the damping between the jointed and control test article due to the joints. This prediction makes use of the previously outlined scheme the results of the finite element analysis, and the measured joint properties.

It is useful to review and verify the assumptions made by the synthesis scheme. They include the assumption that the truss is lightly damped (verified by the measured damping of $\zeta = 0.002$) and the assumption of overall linearity. In static, four-point bending tests of the truss, the load deflection characteristics were found to be very linear, and in dynamic tests no shift in resonance was observed with increasing force level. Over the range of interest, the stiffness and loss factor of the joints were found to be reasonably constant. And implicitly it is assumed that the dynamics of the two test articles are identical, except for the presence of the joints. All static and dynamic comparisons indicated this was so.

The structural loss factor can be estimated from Eq. (17) or calculated using finite element information and Eq. (16). With $N_j = 2$, $N_B = 7$, the joint properties previously discussed, and the tube properties of Table 5, the truss loss factor due to the joints can be estimated from Eq. (17) to be $\eta = 0.0006$, or $\zeta = 0.0003$. By comparison with the measured values of Table 6, which average $\zeta = 0.00043$, this is slightly low. A program was written to perform the more detailed calculation of Eq. (16). The axial strain energy and loss are computed for each bar for a given mode shape and the results summed. Using $\eta_j = 0.01$ and $k_j = 225{,}000$ lb/in., the predicted damping for bending modes 1 and 2 is $\eta = 0.0007$ ($\zeta = 0.0004$) and for torsion mode 3, it is $\eta = 0.0005$ ($\zeta = 0.0003$). Considering the level of damping and difficulty of these measurements, this is remarkable agreement with the measured average of $\zeta = 0.00043$ to 0.00073.

One last calculation was done to estimate the damping, due to losses in the joints in a truss that is completely jointed; i.e., has joints at every node, as will the space station. Predicted damping for the first few modes is $\zeta = 0.001$.

Conclusions

1) If all the features of a structural dynamic model, including such details as the coefficient of friction and tolerances in the joints, are built in perfect replica, and the model is tested at appropriately scaled loads, then the replica model will represent all the nongravitationally induced dynamic features of the full-scale article, including the influences of joint nonlinearity and damping.

2) In certain cases, when the cross-sectional properties of members can be distorted, it is possible to build a multiple-scale, structural dynamic model. This model will correctly represent the dynamics at one scale factor but have the size of a model at a second geometric scale factor. One possible application of such an approach is to set the dynamic scale factor to unity and to choose a smaller geometric scale factor. The resulting model would have exactly the same frequencies as the original article, but be a fraction of its size.

3) In cases where it is not possible to distort the cross sections of small details, such as potentially nonlinear or dissipative joints, these details can be built into a multiple-scale model in replica scale. The resulting scaling laws for such a hybrid-scale model have been derived.

4) Two hybrid-scaled models of a seven-bay segment of the space station truss were built and tested, one that included quick connect joints and a control model that did not. By comparing the measured damping, the contribution of the joints was determined to be between $\zeta = 0.04$ and 0.08%. The use of a jointed and otherwise identical control model was found to be an extremely accurate way in which to isolate the contributions of the joints.

5) The damping synthesis scheme, which incorporated strain distribution information from an undamped, finite element model and experimentally measured joint stiffness and damping data, correctly predicted the magnitude of the structural damping attributable to the joints.

6) Based on the experiments and damping synthesis, it can be estimated that the contribution to the structural damping of the quick connect joints in the space station will not exceed $\zeta = 0.001$.

Appendix: Scaling of Dissipation in Joints

Frictional Joints

Rotary Pin Joint

The layout of a typical pin joint is shown in Fig. 2a. The joint undergoes a local rotation θ when the far end of the tube moves through displacements u and v and is subject to an axial load P and initial distortion in length d_s. The frictional restraining moment at the interface depends on four factors

$$M_F = \mu r_j \left[\left(\frac{EA}{L}\right)_j d_j + \left(\frac{EA}{L}\right)_S d_s + \left(\frac{EA}{L}\right)_S \frac{\partial u}{\partial v} v + Mg \right] \quad \text{(A1)}$$

The first term is due to a geometrically induced preload in a latch or mechanism within the joint, and the second is due to manufacturing tolerances or free thermal deformations d_s causing a preload in the strut. The third is a displacement dependent frictional load,[15] and the fourth is due to gravity loading.

The dissipation caused by this friction in one cycle of motion is

$$\Delta U = 4 \int_0^{\theta_f} M_F \, d\theta \quad \text{(A2)}$$

Assuming that the pin slips such that $\theta_f \sim v/L$, then the dissipation ΔU depends on the scale, as is shown on the first two rows of Table 4. Note that the first three terms of Eq. (12) scale in the same way, whereas the gravity load induced dissipation scales with a higher power of λ.

The validity of the assumption made above that the pin slips in such a way as to have $\theta_f \sim v/L$ must be examined. The equilibrium relation for the slipping pin is

$$\left(\frac{v}{L} - \theta\right) \frac{EI}{L} - M_F = 0 \quad \text{(A3)}$$

from which $\theta L/v$ for equilibrium can be calculated. The manner in which this motion scales is shown in the columns marked "motion" in Table 4.

Extensional Joints

A similar model was developed for the frictional dissipation in a preloading bevel surface joint, typical of quick connect joints under consideration for the space station. Here the preload induced frictional force again depends on four terms:

$$F_F = \mu \left[\left(\frac{EA}{L}\right)_j d_j + c_\beta \left(\frac{EA}{L}\right)_S d_s + k_j u_j \sin\beta + c_\beta Mg \right] \quad \text{(A4)}$$

where c_β is a function of the angle of the contacting surfaces β. Assuming that the joint slip u_j is a fraction of the overall axial motion u, the scale factor for energy dissipation ΔU can be calculated with a relation similar to Eq. (A2) and is shown in Table 4. Again validity, the motion assumption, must be determined by calculating u_j/u from equilibrium:

$$F_F \left(\cos\beta + \frac{1}{\mu} \sin\beta \right) - \left(\frac{EA}{L}\right)_S (u - u_j) = 0 \quad \text{(A5)}$$

The scaling of this motion is shown in the "motion" column of Table 4. For all cases but the gravity induced loads, the dissipation in this axial friction mechanism scales like λ^3, and the normalized slipping motion is independent of λ.

Deadband Impacting Joint

For a simple coefficient of restitution model, with $e = V_f/V_i$, the dissipation in an inelastic collision is

$$\Delta U = \tfrac{1}{2} M v_i^2 (1 - e^2) \quad \text{(A6)}$$

If the frequency of excitation of the overall structure is slow compared to the local dynamics of the joint, then for sinusoidal motion of the far end of the strut, the joint, during the noncontacting portion of a cycle, moves approximately as

$$u_j = \bar{u}_j \sin\omega t \quad \text{(A7a)}$$

$$\bar{u}_j = \frac{\bar{u} EA}{(k_0 + k_1)L} \quad \text{(A7b)}$$

Differentiating to obtain the velocity and evaluating when $u_j = -d$, the time of impact gives

$$\Delta U = \tfrac{1}{2} M \bar{u}_j^2 \omega^2 \left[1 - \left(\frac{d}{\bar{u}_j}\right)^2 \right] [1 - e^2] \quad \text{(A8)}$$

The manner in which this dissipative term scales can now be determined. Under the assumption that the gap d scales like λ, and the coefficient of restitution is unchanged with scale (Table 1), the dissipation scales as shown in Table 4. It is also true that if the gap is scaled as λ, the nonlinear stiffness characteristics are preserved in the scale model.

Acknowledgments

This research was supported by McDonnell Douglas Company with James Peebles as contract monitor and by NASA Headquarters with Samuel Venneri as contract monitor. The contributions from the Lockheed Missile & Space Company were supported by the NASA Langley Research Center with Paul McGowan as contract monitor.

References

[1]Ashley, H., and Edberg, D. L., "On the Virtues and Prospects for Passive Damping in Large Space Structures," Air Force Vibration Damping Workshop II, April 1985.

[2]Balas, M. J., "Trends in Large Space Structures Control Theory: Fondest Hopes-Wildest Dreams," *IEEE Transactions on Automatic Control*, Vol AC-27, No. 3, 1982, pp. 522-535.

[3]Pinson, L. D., and Hanks, B. R., "Large Space Structures Raise Testing Challenges," *Astronautics and Aeronautics*, Vol. 21, No. 10, 1983, p. 34.

[4]Crawley, E. F., and O'Donnell, K. J., "A Procedure for Calculating the Damping in Multi-Element Space Structures," *Acta Astronautica*, Vol. 15, No. 12, 1987, pp. 987-996.

[5]Kuo, C. P., and Wada, B. K., "System Identification of a Truss Type Structure Using the Multiple Boundary Condition Test (MBCT) Method," *Proceedings of the 28th Structures, Structural Dynamics, and Materials Conference*, AIAA, New York, 1987.

[6]Gronet, M. J., Pinson, E. D., Voqui, H. L., Crawley, E. F., and Everman, M. R., "Preliminary Design, Analysis and Costing of a Dynamic Scale Model of the NASA Space Station," NASA CR-4068, July 1987.

[7]Baker, W. E., Westine, P. S., and Dodge, F. T., *Similarity Methods in Engineering Dynamics*, Hayden, Rochelle Park, NY, 1973.

[8]Bisplinghoff, R. L., Ashley, H., and Halfman, R. L., *Aeroelastic-*

ity, Addison-Wesley, Cambridge, MA, Feb. 1955.

[9]Sigler, J. L., Crawley, E. F., and van Schoor, M. C. "Prediction and Measurement of Damping in Hybrid Scaled Space Structure Models," MIT Space Systems Laboratory, Cambridge, MA, Rept. SSL 7-88, 1988.

[10]Crawley, E. F., and O'Donnell, K. J., "Force State Mapping Identification of Nonlinear Joints," *AIAA Journal,* Vol. 25, No. 7, 1987, pp. 1003–1010.

[11]Letchworth, R., McGowan, P. E., and Gronet, M. J., "COFS III, Multibody Dynamics and Control Technology," *Proceedings of NASA/DOD Control/Structures Interaction Technology Conference,* NASA CP 2447, Pt. 2, Nov. 1986.

[12]Sarver, G. L., and Crawley, E. F., "Energy Transfer and Dissipation in Structures with Discrete Nonlinearities," MIT Space Systems Laboratory, Cambridge, MA, Rept. SSL 25-87, 1987.

[13]Bowden, M., "Dynamics of Space Structures with Nonlinear Joints," MIT Space Systems Laboratory, Cambridge, MA, Rept. SSL 15-88, 1988.

[14]Keinholz, D. A., and Allen, B. R., "Force State Testing of a Quick Connect Joint," CSA Engineering, Palo Alto, CA, Rept. 87-02-01, Feb. 1987.

[15]Hertz, T. J., and Crawley, E. F., "Displacement Dependent Friction in Space Structure Joints," *AIAA Journal,* Vol. 23, No. 12, 1985, pp. 1998–2000.